Evaluation of surface shortwave downward radiation forecasts by the numerical weather prediction model AROME

Marie-Adèle Magnaldo, Quentin Libois, Sébastien Riette, and Christine Lac

CNRM, Université de Toulouse, Météo-France, CNRS, Toulouse, France

Correspondence: Quentin Libois (quentin.libois@meteo.fr)

Abstract. With the worldwide development of the solar energy sector, the need for reliable surface shortwave downward radiation (SWD) forecasts has significantly increased in recent years. SWD forecasts of a few hours to a few days based on numerical weather prediction (NWP) models are essential to facilitate the incorporation of solar energy into the electric grid and ensure network stability. However, SWD errors in NWP models can be substantial. In order to characterize the performances of AROME in detail, the operational NWP model of the French weather service Météo-France, a full year of hourly AROME forecasts is compared to corresponding in situ SWD measurements from 168 high-quality pyranometers covering France. In addition, to classify cloud scenes at high temporal frequency and over the whole territory, cloud products derived from the Satellite Application Facility for Nowcasting and Very Short Range Forecasting (SAF NWC) from geostationary satellites are also used. The 2020 mean bias is positive, with a value of $18\,\mathrm{W\,m^{-2}}$, meaning that AROME on average overestimates the SWD. The root-mean-square error is $98\,\mathrm{W\,m^{-2}}$. The situations that contribute the most to the bias correspond to cloudy skies in the model and in the observations, situations that are very frequent (66 %) and characterized by an annual bias of $24\,\mathrm{W\,m^{-2}}$. Part of this positive bias probably comes from an underestimation of cloud fraction in AROME, although this is not fully addressed in this study due to the lack of consistent observations at kilometer resolution. The other situations have less impact on SWD errors. Missed cloudy situations and erroneously predicted clouds, which generally correspond to clouds with a low impact on the SWD, also have low occurrence (4 % and 11 %). Likewise, well-predicted clear-sky conditions are characterized by a low bias ($3\,\mathrm{W\,m^{-2}}$). When limited to overcast situations in the model, the bias in cloudy skies is small ($1\,\mathrm{W\,m^{-2}}$) but results from large compensating errors. Indeed, further investigation shows that high clouds are systematically associated with a SWD positive bias, while low clouds are associated with a negative bias. This detailed analysis shows that the errors result from a combination of incorrect cloud optical properties and cloud fraction errors, highlighting the need for a more detailed evaluation of cloud properties. This study also provides valuable insights into the potential improvement of AROME physical parametrizations.

1 Introduction

In the context of global warming, the European Union's Green Deal calls for at least 45 % of energy to come from renewable energy sources (RESs) by 2030. This is expected to reduce greenhouse gas emissions by 55 % compared to 1990 levels (https://energy.ec.europa.eu/topics/renewable-energy/renewable-energy-directive-targets-and-rules/renewable-energy-targets_en, last access: 25 April 2023). The share of RESs has already increased significantly in Europe and worldwide over the last decade (International Energy Agency, 2019). In France, in 2021, 13 067 MWp (MW peak) of solar photovoltaic (PV) generation capacity was installed (which corresponds to the potential production under standard test conditions), and 2687 MWp was added in 2021 (Réseau de transport d'électricité, 2021). Solar energy covers 3.1 % of the French annual electricity consumption (https://bilan-electrique-2021.rte-france.com/production_solaire/, last access: 25 April 2023). This highlights that solar energy is a key element in moving to a more sustainable energy system.

However, solar energy production is highly dependent on weather conditions, especially clouds, which are responsible for its very high spatiotemporal variability (Widén et al., 2015; Antonanzas et al., 2016). This variability is an issue for the planning of solar energy production and for the overall stability of the electric grid, which requires a balance between supply and demand (Antonanzas et al., 2016; Betti et al., 2021). To deal with that, accurate forecasts, mainly for surface shortwave downward radiation (SWD), are essential. Different forecasting horizons are relevant for the solar energy sector, ranging from minutes to months ahead (Das et al., 2018; Antonanzas et al., 2016; Raza, 2016; Betti et al., 2021). Very short term forecasts, covering horizons from seconds to 1 h, are important for power smoothing, real-time electricity dispatch and the optimization storage. Short-term forecasts, from 1 h to several days, are necessary for unit commitment, scheduling and dispatch of electrical power, and also the enhancement of the security of grid operation. Medium-term forecasts, from 1 week to 1 month, are useful, for example, for scheduling maintenance. Long-term forecasts, from 1 month to 1 year, are useful for planning electricity generation, transmission and distribution aside from energy bidding and securing operations (Das et al., 2018). In the much longer term, in particular in the context of global warming, estimating the future potential of variable renewable resources, including solar, and the impact of temperature on electricity demand is essential to provide an assessment of future energy systems (Dubus et al., 2022).

Depending on the time horizon, different forecasting techniques are used (Widén et al., 2015; Raza, 2016; Das et al., 2018; Betti et al., 2021). For instance, for intra-hour forecasts, the use of two or more all-sky imagers (ASIs) organized in a network has proven successful (Nouri et al., 2019b, a; Logothetis et al., 2022; Chu et al., 2022). Forecasting techniques based on historical data, including machine learning approaches, can also be effective for the very short term (Das et al., 2018). For short-term forecast up to 6 h horizon, satellite-based methods that extrapolate cloud location using cloud-motion vectors can be effective (e.g., Cros et al., 2020). From hours to a few days, physical methods based on weather forecasts produced by numerical weather prediction (NWP) models are the most common (Widén et al., 2015; Antonanzas et al., 2016; Betti et al., 2021). As a consequence, these NWP models, which solve the mesoscale atmospheric dynamics and account for small-scale physical processes, are an essential element for the management of power systems involving a significant amount of solar energy.

However, the performance of NWP models in predicting SWD remains limited. As an illustration, we compared the 1 d SWD forecasts of AROME (Seity et al., 2011), the operational NWP model of the French weather service Météo-France, to hourly averages from the national pyranometer network comprising 168 stations. For 2020, the mean annual bias and root-mean-square error (RMSE) are respectively 18

and 97 W m^{-2}, for a mean SWD of 340 W m^{-2}. This shows that the errors can be significant, with correspondingly high uncertainties in the PV production forecasts.

Nevertheless, until now, SWD errors have not been a priority for weather forecasts produced by NWP models, since they did not have radiative scores, whereas they have been particularly studied in climate models. Growing interest from various end users, including the PV community, is now highlighting these substantial SWD errors and the need for better forecasts.

For example, Nielsen and Gleeson (2018) evaluated the SWD forecasts of the NWP model HARMONIE-AROME in Denmark with a pyranometer network and found a negative bias for days with optically thick clouds, which they attributed to an excess of cloud water in the model thick clouds. This approach is interesting because it allows a model to be evaluated over a large domain and a long period, but it does not distinguish between cloud regimes such as cloud altitude or phase, which could help better understand SWD errors. Köhler et al. (2017) had a different approach, allowing for a distinction by cloud regime. They analyzed the PV power forecast errors of the NWP model COSMO-DE in Germany for 2013 and 2014 and highlighted that nearly one-third of the 100 d with the largest SWD errors was associated with fog and low stratus events. However, while this study demonstrated the need for more reliable forecasts of low cloud cover, it was limited to 100 d and the cloud regimes were analyzed manually, which did not allow a systematic distinction of cloud situations. Other more systematic studies relied on highly instrumented sites with lidars and radars to detect the presence of clouds (Tuononen, 2019), or to automatically classify clouds based on their base and thickness (Ahlgrimm and Forbes, 2012). These approaches are useful for determining how cloud regimes and cloud physical parameters contribute to SWD errors in NWP models. More specifically, Tuononen (2019) showed that low and mid-level clouds in the Integrated Forecast System (IFS) model in Helsinki are associated with a positive bias of SWD when the liquid water path (LWP) is low. They showed that an overestimation of SWD correlates with an underestimation of cloud fraction in the IFS model. Similarly, Ahlgrimm and Forbes (2012) estimated that at the ARM Southern Great Plains (SGP) site, in overcast low cloud conditions, the frequency of low-LWP clouds was overestimated, and the frequency of high-LWP clouds was underestimated in the IFS model.

These highly instrumented sites also allow other parameters to be evaluated in the absence of clouds. For instance, at the ARM SGP site, Weverberg et al. (2018) analyzed the contributions of surface albedo, surface longwave emission, integrated water vapor, aerosols and cloud properties in nine global circulation models and found that cloud errors generally dominate SWD errors. Likewise, Morcrette (2002) found an underestimation of water vapor absorption and errors in humidity and in aerosol concentrations in the IFS model. Rieger et al. (2017) also reported large SWD errors during

a Saharan dust outbreak over Germany in the ICON NWP model.

While most studies investigating the causes of SWD errors in NWP forecasts have used highly instrumented sites where detailed, high-frequency observations are available, this approach remains limited to a single site. In our study, we aim to develop a general method to evaluate SWD forecasts from NWP models and identify the situations that contribute most to errors. The method should allow a large domain to be dealt with, with a sufficient number of reference observations, as in Nielsen and Gleeson (2018). Hence, it should not be limited to a single supersite because such a site could be unrepresentative of the whole domain. The method should also allow us to go further in identifying cloud errors. Our strategy is also to explore a wide variety of meteorological situations, which is possible by evaluating the model throughout the year and not only during a short period where specific seasonal errors could dominate the overall behavior. Finally, our method is intended to be general and systematic enough to be applied to any NWP model, relying only on SWD observations and making extensive use of cloud satellite products.

In this paper, our evaluation methodology is applied to AROME at 1.3 km horizontal resolution. For this purpose, a full year of 1 d hourly forecasts is compared with in situ SWD measurements from the pyranometer network operated by Météo-France. The cloud products derived from the Satellite Application Facility for Nowcasting and Very Short Range Forecasting (SAF NWC) from geostationary satellites are used to classify cloud scenes at high temporal frequency and over the whole territory.

The paper is organized as follows. Section 2.1 presents the SWD measurements and the satellite products, as well as the AROME forecasts used in this study. The evaluation methodology is then detailed in Sect. 2.2. Section 3 presents the results, first in terms of cloud occurrence and then in terms of cloud situations. The results are then put into perspective in Sect. 4, where the limitations of the observations and potential sources of error in AROME are discussed.

2 Data and methods

2.1 Observation and modeling data

2.1.1 AROME forecasts

AROME (Applications de la Recherche à l'Opérationnel à Méso-Echelle) is a limited-area non-hydrostatic model developed by the French weather service, Météo-France (Seity et al., 2011; Brousseau et al., 2016). The French operational configuration of AROME covers a large part of western Europe and has a horizontal resolution of 1.3 km. The number of model pixels is 1525×1429, and the number of vertical levels is 90. The time step is 50 s. The lateral boundary conditions are provided by ARPEGE (Action de Recherche Petite

Echelle Grande Echelle), the French operational global NWP model.

The AROME model physical package is derived from the Meso-NH model (Lafore et al., 1998; Lac et al., 2018). The shallow convection is parametrized using the EDMF (Eddy Diffusivity Mass Flux) approach (Pergaud et al., 2009). The microphysical scheme is the one-moment mixed ICE3 scheme, completed with a subgrid condensation scheme presented in Riette and Lac (2016). The turbulence parametrization considers a prognostic turbulent kinetic energy (TKE) equation from the Cuxart et al. (2000) scheme in a 1D mode and is closed with the Bougeault and Lacarrere (1989) mixing length. The radiation parametrization comes from the IFS model and comprises the six spectral bands' shortwave radiation scheme of Fouquart and Bonnel (1980) and the Rapid Radiative Transfer Model for longwave radiation (Mlawer et al., 1997). AROME is coupled online with the SURFEX (externalized land and ocean surface platform) model, which describes the surface fluxes and the evolution of four types of surfaces: natural, town, inland water and ocean (Masson et al., 2013).

In this study, 24 h operational hourly forecasts starting at 00:00 UTC are evaluated, considering the average hourly SWD and average hourly total cloud fraction forecasts. We also use the average hourly cloud fraction in slices across the tropospheric column, located at pressure levels 1013–785 hPa (~ 2 km), 785–450 hPa (~ 6 km) and 450 hPa–top of the model. This study focuses on the year 2020 (corresponding to the AROME cycle 43t1). This year was chosen because it corresponds to a recent and continuous period without major changes in the AROME operational model.

2.1.2 Observations of shortwave downward radiation

Within the operational observation network of Météo-France, 221 pyranometers in mainland France provide hourly means of SWD. Among them, only 168 were used during the whole year 2020 and considered of sufficient quality. Their locations are shown in Fig. 1. Practically, measurements taken under critical environmental conditions (e.g., with significant local masks or in mountainous regions above 1000 m) or with time series showing anomalies have been discarded to avoid introducing observational errors in the reference measurements.

2.1.3 Cloud satellite products

In order to identify the presence and type of clouds at high frequency and over the whole AROME domain, cloud satellite products developed by the NWC EUMETSAT SAF are used (LeGleau, 2019; LeGléau and Kerdraon, 2019). Over France, the horizontal resolution is around 5 km, and the temporal frequency is 15 min, so there are four values for 1 h. The cloud mask product gives discrete values: 0 for no cloud and 1 for clouds. The cloud type is a classification among 15
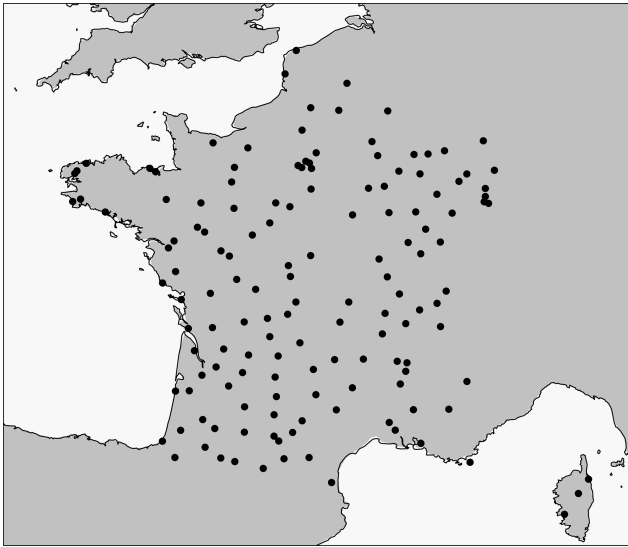
Figure 1. Localization of the 168 pyranometers used from the network operated by Météo-France.

different classes: 4 corresponding to cloud-free scenes and 11 corresponding to cloud scenes (see Sect. 2.2.3).

2.2 Methods

2.2.1 Model–observation comparison of shortwave downward radiation

We compare hourly means of SWD from the model and from observations. To avoid grazing angles under which pyranometer measurements can be inaccurate, only the diurnal values corresponding to a cosine of the solar zenith angle (SZA) greater than 0.1 (equivalent to a SZA less than 84.3°) are considered. To avoid double-penalty issues, usual for high-resolution models like AROME that are unlikely to form clouds at exactly the right place and time (Amodei and Stein, 2009; Stein and Stoop, 2019), we do not necessarily select the closest point, unlike most SWD evaluation studies, but instead extract it in the vicinity of the observation point. In practice, a neighborhood strategy is set up that allows the selection of a model point with a forecast SWD value close to the observed value in a small square domain centered on the observation point. While such a neighborhood strategy may seem unsatisfactory to PV producers who are concerned about SWD at the exact location of the PV plant, these users should keep in mind that NWP forecasts are not expected to be accurate at individual grid points. We sort the absolute model–observation errors in this neighborhood in ascending order and select the 10th percentile value. This strategy avoids the selection of a point very close to the observation by chance and ensures that the method is not too sensitive to the size of the neighborhood. Here, the size of the neighborhood is set to 5×5 model pixels, which means

that the point with the second smallest difference (among 25 values) is retained for each observation. The neighborhood size is chosen to be comparable to the satellite pixel size (see Sect. 2.2.2).

The error metrics commonly used to evaluate the SWD forecast errors are the mean error or bias (ME) and the root-mean-square error (RMSE). The ME describes systematic deviations and provides information on the sign of error. However, the ME is not sufficient to assess errors because of compensation effects. The RMSE is more sensitive to large errors and thus particularly suited to the electricity market, where large errors are much more critical than small errors (Perez et al., 2013; Betti et al., 2021). The RMSE can be divided into systematic errors (MEs) and unsystematic errors or standard deviation of errors (SDE), as described in Widén et al. (2015):

$$\mathrm{RMSE}^2 = \mathrm{SDE}^2 + \mathrm{ME}^2. \tag{1}$$

In practice, while it can be relatively easy to correct the bias in a model, with a simple tuning or a statistical adjustment, reducing SDE is generally more challenging.

2.2.2 Cloud occurrence classification

To identify cloud presence in the observations, we use the satellite cloud mask. As AROME forecasts are only available as hourly means, comparable satellite products at hourly resolution are computed. Clear-sky conditions are considered for a pyranometer location (i.e., the satellite pixel including the location of the pyranometer) at hour H when the last four consecutive observations report no clouds. To identify clear-sky conditions in AROME, the hourly mean total cloud fraction is computed as the average over the neighborhood defined in the previous section. A threshold value of 2 % is fixed: if the hourly mean total cloud fraction is larger than this value, the hour is considered cloudy and clear sky otherwise. Once cloudy skies are identified in both observations and the model, we set up a contingency table, following Tuononen (2019): "hit" when clouds are present in the model and in the observation, "false alarm" when clouds are present in the model only, "miss" when clouds are present in the observation only, and "correct negative" when both observations and the model agree on clear-sky conditions.

2.2.3 Cloud regimes and cloud types

In the model, to further discriminate between different cloudy situations, we use a modeled cloud regime classification similar to Weverberg et al. (2018). In AROME forecasts, the cloud fraction for each of the three distinct vertical slices is used. For each region, a 2 % threshold, similar to the threshold value for cloud occurrence, is set to distinguish cloudy and clear-sky conditions. The value of this threshold is the same as the threshold value for cloud occurrence classification (see Sect. 2.2.2). Seven cloud regimes (CR1 to 7) are
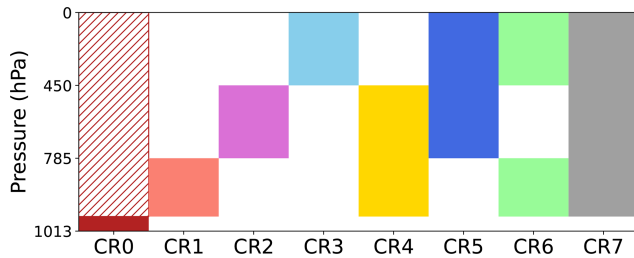
Figure 2. Modeled cloud regime classification.

defined from the combination of these cloudy layers. When the liquid water content is larger than $10^{-5}\,\mathrm{kg\,kg^{-1}}$ at the first vertical level of the model, the cloud regime is set to CR0, which corresponds to fog. These eight cloud regimes are depicted in Fig. 2. Table 1 summarizes the different naming used to describe groups of cloud regimes used in this article.

In the observations, to further distinguish cloudy skies, we use a cloud type classification based on the cloud type satellite product developed by SAF NWC and described in Sect. 2.1.3. As the values are instantaneous and discrete, we select the values at $H-30$ min. The 11 cloud types of the product are merged into 6 (Table 2), allowing an easier comparison with model outputs.

Figure 3 shows the monthly relative frequency for each cloud regime (respectively type) and for the clear skies in the model (respectively in the satellite product) over the pyranometer locations and when $\cos(\mathrm{SZA}) > 0.1$. In the model, the frequency of clear skies is 22 % against 30 % in the satellite product, suggesting that the model predicts too many clouds, and/or some optically thin clouds are not detected by the NWC SAF product, which is a known caveat of passive sensors (Sun et al., 2011). AROME predicts fewer low clouds (23 % of CR0+CR1+CR4) than satellite observations (29 % of LCs). In addition, the relative frequency of observed fractional clouds is higher in summer than in winter, while low clouds are overall less frequent in spring and summer, highlighting seasonal cycles in the observations that do not have obvious equivalents in the model. We can also note that the model predicts too many thick clouds with a high cloud top (29 % of CR5+CR7) compared to the observations (9 % of HCs). Note that the sum of the relative frequencies of clear skies and all cloud regimes is not exactly equal to 1 in Fig. 3a. This is because there are situations with very low relative frequencies with a total cloud fraction larger than 2 % (implying that the scene is considered cloudy) but with a cloud fraction for each of the three vertical slices of the troposphere lower than 2 % (implying that it is not associated with any CR).

3 Statistical analysis

The method presented in the previous section is now applied to evaluate the AROME SWD forecasts, starting with an overall evaluation before going into detail.

3.1 Overall evaluation: clear-sky index histograms

To begin with, we use the clear-sky index (CSI), which is defined as

$$\mathrm{CSI_{mod}} = \frac{\mathrm{SWD_{mod}}}{\mathrm{SWD_{clear,mod}}} \; ; \; \mathrm{CSI_{obs}} = \frac{\mathrm{SWD_{obs}}}{\mathrm{SWD_{clear,mod}}}, \qquad (2)$$

with $\mathrm{SWD_{mod}}$ the SWD in the model, $\mathrm{SWD_{obs}}$ the SWD in the observations, and $\mathrm{SWD_{clear,mod}}$ the theoretical SWD under clear-sky conditions from the model. The histograms of CSI are used to point differences in SWD between AROME and observations (Fig. 4), similarly to what Nielsen and Gleeson (2018) did to evaluate the NWP model HARMONIE-AROME against the Danish pyranometer network. The CSI roughly quantifies overall cloud transmittance, bearing the signature of both cloud cover and cloud optical thickness. Only values for which the SZA is less than 70° are considered to ensure that the CSI distribution is not affected by measurement errors and model limitations at grazing angles.

In the observations the CSI can greatly exceed 1, as reported by Nielsen and Gleeson (2018). This can be explained by an underestimation of the model clear-sky SWD, which can be due to a reduction in aerosol emissions over the last decades (Wild, 2009), while the aerosol climatology used in AROME is older (Tegen et al., 1997) and thus overestimates present-day aerosol loadings. These values exceeding 1 can also be due to cloud enhancement effects (e.g., Gueymard, 2017), which occur under broken cloud conditions. Such effects cannot be simulated with standard plane-parallel radiative codes (Wissmeier et al., 2013). The few CSI values in the model exceeding 1 are unrealistic and are due to the fact that the theoretical SWD under clear-sky conditions from the model is slightly delayed compared to the SWD. The CSI in the model is more frequently between 0.8 and 1 compared to observations (which may partly be due to the lack of values exceeding 1 in the model), or less than 0.1, and in contrast less frequently between 0.1 and 0.75. It suggests that optically thick clouds are too thick, which agrees with the excess of CR5 and CR7 pointed in Fig. 3. Interestingly the CSI distributions are similar to those reported by Nielsen and Gleeson (2018) with HARMONIE-AROME (Bengtsson et al., 2017). Although these models share the same code, the operational configurations rely on different sets of parametrizations. It suggests that NWP model errors are to some extent systematic over a wide range of situations. The opposite behaviors in different ranges of CSI show that errors in AROME are not limited to a systematic bias, which could be easily corrected with a rough tuning. Instead, the behaviors seem to depend on the cloud situation, which will be investigated further in the following.

Table 1. Table summarizing the different naming used to describe groupings of cloud regimes used in this article.

Low clouds	Cloud regimes with clouds present in the lower vertical slices: CR0, CR1 and CR4
High clouds	Cloud regimes with clouds present in the upper vertical slices (except CR6): CR3, CR5 and CR7
Geometrically thin clouds	Cloud regimes with clouds present in only one vertical slice: CR1, CR2 and CR3
Geometrically thick clouds	Cloud regimes with clouds present in two or more vertical slices (except CR6): CR4, CR5 and CR7

Table 2. Observed cloud type classification.

LC	Low clouds, which include very low and low clouds
MC	Mid-level clouds, which include mid-level clouds
SC	Semi-transparent clouds, which include high semi-transparent thin clouds, high semi-transparent moderately thick clouds, high semi-transparent thick clouds, high semi-transparent above low or medium clouds, and high semi-transparent above snow/ice
HC	High clouds, which include high opaque clouds and very high opaque clouds
FC	Fractional clouds, which include fractional clouds
Others	Fill values or when the cloud type product indicates no clouds unlike the cloud mask product

3.2 Attributing model errors to cloud occurrence

To go beyond Fig. 4, we now investigate how the different cases of cloud presence defined in Sect. 2.2.2 contribute to the overall errors. To this end we compute the relative frequency, SWD bias and SDE for each of the four occurrence cases. To identify the situations that contribute most to errors, another metric is used: the contribution to the total bias, which is the frequency-weighted bias. The sum of these contributions equals the total bias. If a situation is associated with a high bias but rarely occurs, it barely contributes to the total bias. In contrast, a situation associated with a low bias can significantly contribute to the total bias if it frequently occurs. Figure 5a shows the monthly bias, frequency and contribution to the total bias.

As expected, the bias is negative for the false alarm cases (ranging from -5 to $-25\,\mathrm{W\,m^{-2}}$), and positive for the miss cases (with monthly biases up to $80\,\mathrm{W\,m^{-2}}$). The false alarm cases are almost 3 times more frequent than miss cases (11 % of false alarm cases and 4 % of miss cases during the year 2020), which is consistent with the higher clear skies frequency in the observations pointed in Sect. 2.2.3 and suggests that AROME predicts too many clouds or that some clouds are not detected by the satellite. With a cloud fraction threshold value of 10 %, the gap between the two frequencies is reduced, but false alarm cases remain more frequent (10 % of false alarm cases and 6 % of miss cases). The bias is stronger for the miss cases than for the false alarm cases. This suggests that clouds missed by AROME have more impact on the SWD than those simulated in false alarm cases

or that some false alarm cases are actually hit cases with undetected clouds. When both the model and observations predict clear skies, the bias is much smaller, ranging from -10 to $10\,\mathrm{W\,m^{-2}}$, and is on average slightly positive during the year. The hit cases represent 66 % of the situations and are associated with significant biases up to $50\,\mathrm{W\,m^{-2}}$. Their contribution to the total bias is the most important ($16\,\mathrm{W\,m^{-2}}$, for a total bias of $18\,\mathrm{W\,m^{-2}}$). Interestingly, the bias associated with hit cases is invariably positive throughout the year, showing a marked tendency of AROME to underestimate the impact of clouds on the SWD. Figure 5b shows that the SDE is also the strongest for the hit cases, with annual values of $110\,\mathrm{W\,m^{-2}}$, compared to $50\,\mathrm{W\,m^{-2}}$ for the false alarm cases, $95\,\mathrm{W\,m^{-2}}$ for the miss cases and $22\,\mathrm{W\,m^{-2}}$ for the correct negative cases. Note that several tests were performed by changing the neighborhood size (1 pixel and 10×10 pixels), the cloud detection threshold (1 %, 5 %, 10 %) and the SZA threshold (70°), which did not qualitatively change these results. Hence we consider these results are robust and independent of the mentioned thresholds. To summarize, errors mostly occur when clouds are present in the model and in the observations, which is consistent with Weverberg et al. (2018) and Tuononen (2019).

3.3 Attributing model errors to AROME cloud regimes and satellite cloud types

In what follows, we provide a more physical overview of correct negative cases, false alarm cases and miss cases results. Then we focus more extensively on the hit cases that con-
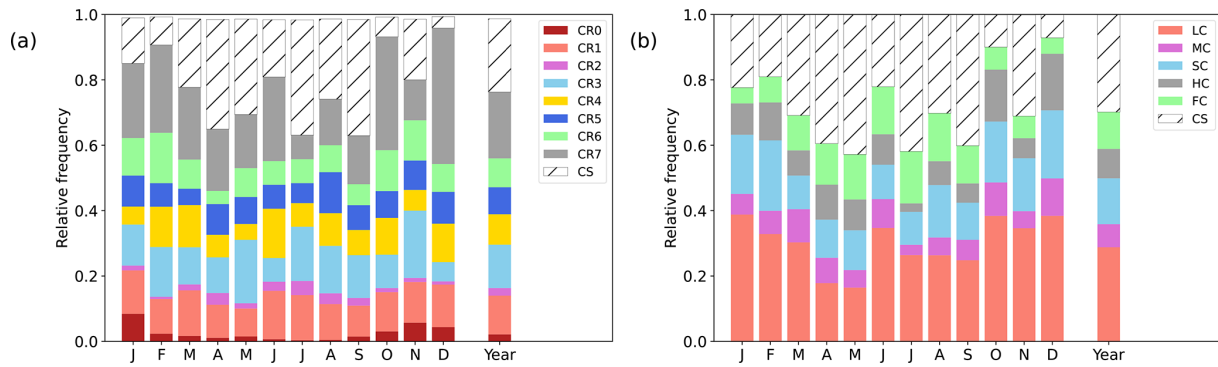
Figure 3. Monthly relative frequency for each **(a)** cloud regime in AROME and clear skies (CS) and **(b)** cloud type in the satellite images and clear skies (CS), over 2020 for the pixels including the pyranometers.
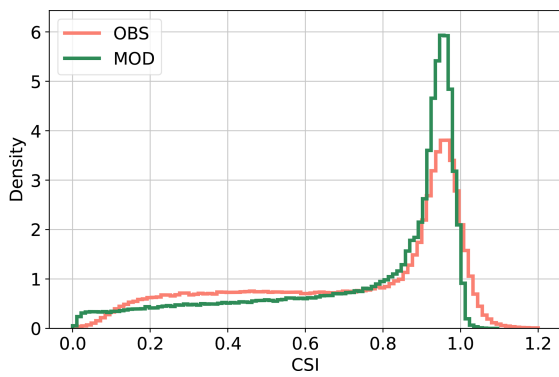

Figure 4. Clear-sky index distribution in the model and in the observations when SZA > 70° over 2020.

tribute most to SWD errors. To this end, we distinguish between situations in terms of cloud regimes in AROME or in terms of the satellite cloud types, so that bias and SDE can be attributed to these specific cloud situations.

3.3.1 Correct negative cases

Various factors can explain SWD errors for the correct negative cases. For example, Morcrette (2002) found a persistent positive bias in clear sky that was attributed to an underestimation of gaseous absorption in the IFS water vapor spectroscopy, which is still the one used in AROME. Another factor which can contribute to SWD errors in clear-sky condition is relative to aerosols. In AROME, the aerosols are prescribed by a monthly climatology (Tegen et al., 1997), meaning that only the average seasonal cycle of aerosols is captured, but the individual aerosol events are not accounted for. Such events, for instance dust outbreaks, can result in localized SWD attenuation of 40 %–50 %, as pointed out by Kosmopoulos et al. (2017), so not taking them into account can lead to significant SWD errors (Rieger et al., 2017).

To estimate the extent to which such a misrepresentation of aerosols contributes to the errors of the correct nega-
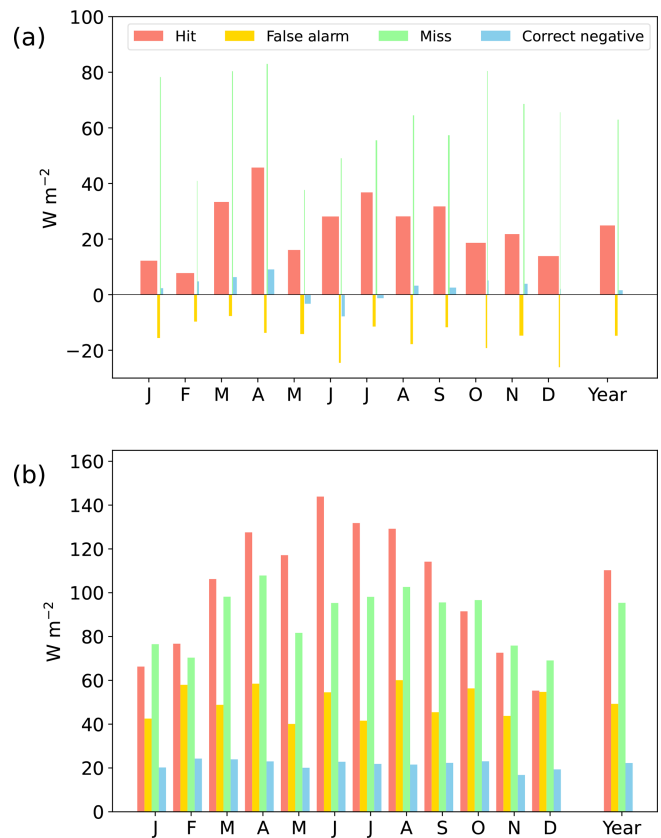

Figure 5. (a) Monthly mean SWD bias (bar height, in $W\,m^{-2}$) and relative frequency (bar width) for each category during the year 2020: red for the hit cases, yellow for the false alarm cases, green for the miss cases and blue for the correct negative cases. The total contribution is the bar surface. **(b)** Monthly SWD standard deviation of errors (SDE) for each category during the year 2020.

tive cases, we examine the correlation between SWD errors and aerosol optical depth (AOD) errors, the latter being defined as the difference between the climatological AOD from AROME and the AOD estimated from Copernicus Atmo-

sphere Monitoring Service (CAMS), a chemistry-transport model that provides near-real time AOD forecasts and fully captures aerosol-related events (Benedetti et al., 2009; Morcrette et al., 2009), interpolated to the AROME grid. Figure 6 shows the natural logarithm of the transmittance (defined as $T = \text{SWD}/\text{SWD}_{\text{TOA}}$ with SWD_{TOA} the SWD at the top of the atmosphere) errors as a function of AOD errors divided by cos(SZA) in the correct negative cases, as well as the linear regression line. Again, only values for which the SZA is less than 70° are considered in order to avoid values of SWD_{TOA} that are too low.

As expected, a negative slope is obtained during the year 2020 with a value of −0.07 and also for each individual month (not shown). The correlation coefficient is low, showing a large variability in the data, with a value of −0.19 during the year and less negative values in winter and higher values in summer. However, throughout the year the p value is very low, indicating a statistically significant relationship between SWD errors and AOD errors. The low correlation coefficient could be explained by the different factors mentioned above that explain SWD errors but mainly by clouds which are not detected by cloud products but alter the SWD (see Sect. 4.1.2). Using passive measurements for cloud detection limits our study of aerosol errors because cloud detection errors influence clear-sky SWD errors at the first order. A better cloud detection is required to identify real clear skies in reality, as discussed in Sect. 4.1.2.

We do not extend further on these clear-sky cases which have been treated elsewhere, notably Rieger et al. (2017), who show an overall improvement of the PV-power forecast during a Saharan dust event over Germany in the ICON model when extended with modules accounting for trace gases and aerosols and related feedback processes. Moreover, the Tegen climatology used in AROME is outdated, and a more recent climatology such as the CAMS climatology could reduce SWD errors, as implemented in the IFS (Bozzo et al., 2020).

3.3.2 False alarm cases

False alarm cases correspond to clouds predicted by AROME but not observed by the satellite. Here we study the type of clouds present in AROME in such cases in more detail. Figure 7a shows that the relative frequency for geometrically thin clouds in AROME, designating cloud regimes with clouds in only one vertical slice of the troposphere, is higher when no clouds are detected than in the AROME total cloud climatology (for instance 50 % vs 18 % for CR3; see Fig. 3a). This suggests that some thin clouds (mostly high clouds) predicted by AROME are not physically realistic or are not detected by the satellite. Regarding the biases, they are mostly negative for most of the cloud regimes, except for CR3 for a few months, CR3 having the lowest absolute bias throughout the year. This also shows that some geometrically thin high clouds may not be detected. The major contribution to
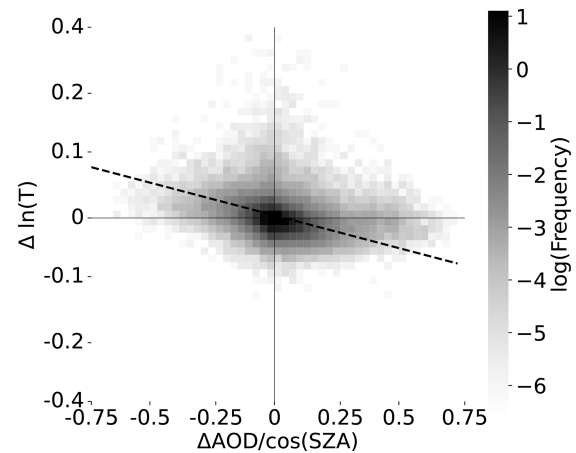

Figure 6. $\ln(\text{SWD}/\text{SWD}_{\text{TOA}})$ errors as a function of AOD errors with the fit line during clear skies in the year 2020 when the SZA is less than 70°.

the total bias in false alarm cases is for geometrically thin low clouds (CR1) which have a lower frequency than CR3 but a much larger bias throughout the year. Given the SWD errors associated with CR1, it is likely that some are erroneously predicted by the model. In contrast, almost no geometrically thick clouds (CR4, CR5 and CR7) are simulated when no clouds are observed (5 % for CR4, 6 % for CR5 and 2.7 % for CR7), while they are predominant in the total climatology (13 % for CR4, 11 % for CR5 and 28 % for CR7). This is consistent with the fact that simulating thick clouds in the absence of clouds is unlikely and that thick clouds are less likely to be undetected. Note that the annual mean SWD in the model for the false alarm cases (436 W m^{-2}) is much higher than the annual mean SWD in the model for the hit cases (296 W m^{-2}), suggesting that undetected simulated clouds have on average less impact on the SWD than actually observed clouds.

Around 4 % of the false alarm cases are fog, compared to about 3 % of simulated clouds in total. In winter, there can be up to 3 times more fog in the false alarm cases than in the total AROME cloud climatology, suggesting that during the day in winter, there is a lot of simulated fog, while no cloud is detected. As fogs are largely present in the morning (7.6 % in the morning and 0.5 % in the afternoon during the year), this may be due to the delay in dissipation of AROME fog highlighted by Antoine et al. (2023). In winter, the highest negative bias is for fog (minimum of −83 W m^{-2}) with a relatively high frequency, showing that the contribution of fog to the bias is particularly important in winter and that improving AROME fog forecasts is an important issue for SWD errors.

3.3.3 Miss cases

As for the false alarm cases, the objective is to identify which cloud types have been missed by AROME. Figure 7b shows
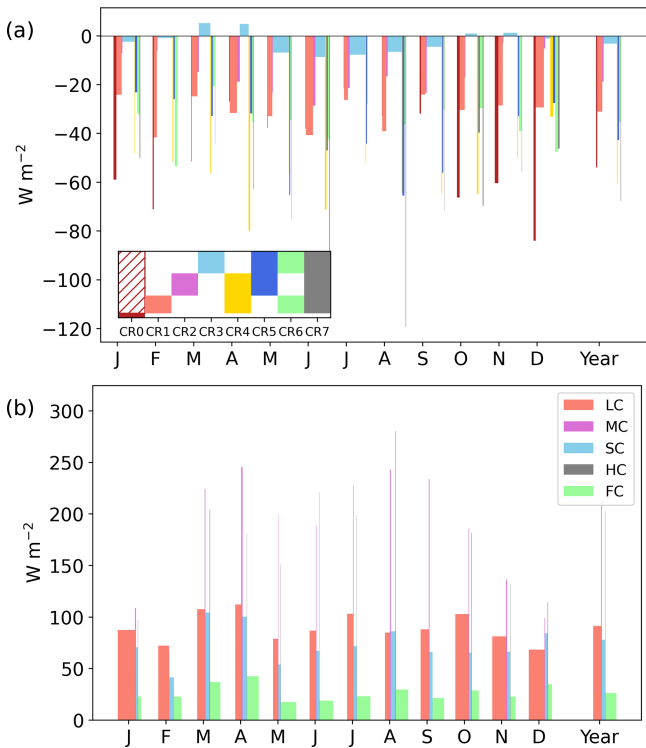
Figure 7. Monthly bias (bar height) and relative frequency (bar width) for **(a)** each cloud regime for the false alarm cases and **(b)** each cloud type for the miss cases. The vignette of the cloud regimes is inserted to facilitate the reading.

Figure 8. Monthly mean SWD bias (bar height, in $W\,m^{-2}$) and relative frequency (bar width) for each **(a)** cloud regime and **(b)** cloud type, during the year 2020 for the hit cases. The total contribution is the bar surface.

that the seasonal cycle is more pronounced than for the false alarm cases. In winter, the relative frequency of low clouds (LCs) in the miss cases is much higher (maximum of 74 %) than for the observed climatology as a whole (41 %; see Fig. 3b), while the opposite is true in summer with a minimum of 21 %. Figure 7b also shows that, as expected, the bias for all cloud types is positive and that the main contribution to the bias for the year 2020 comes from LC, especially in winter and autumn.

The annual relative frequency of fractional clouds (FCs) in miss cases is the highest (47 %), especially in summer when they are more frequent with a maximum of 67 %. Regardless of the season, the relative frequency of FC in miss cases is higher than in the total observed climatology (maximum of 27 %).

Few high clouds (HCs) are missed, with an annual relative frequency of 1 % (13 % in the total observed climatology), unlike semi-transparent clouds (SCs), which are often missed with an annual relative frequency of 14 % (20 % of the total observed climatology). The highest biases come from mid-level clouds (MCs) (211 $W\,m^{-2}$) and HCs (203 $W\,m^{-2}$), but due to their very low occurrence, their contribution to the bias in miss cases is very small, in contrast to SC. Note that the annual mean SWD in the observations for miss cases (409 $W\,m^{-2}$) is much higher than for hit cases (272 $W\,m^{-2}$),
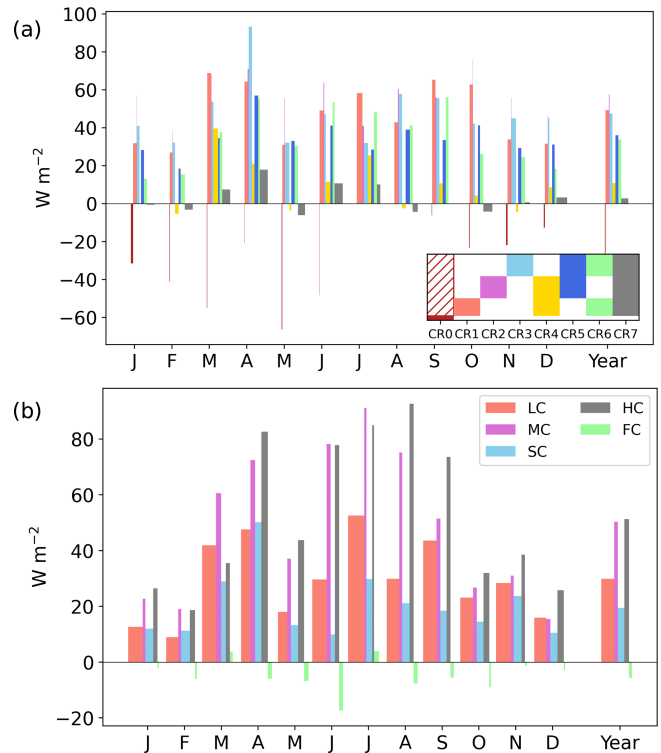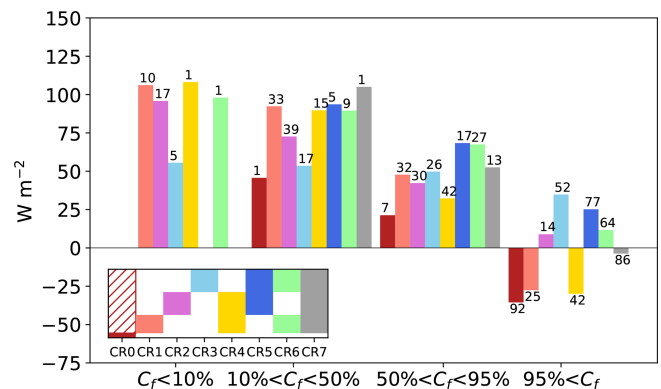

Figure 9. Annual mean SWD bias for different AROME cloud fractions and for each cloud type during the year 2020. The number above each bar represents the frequency (in %) by cloud fraction range for each cloud regime.

suggesting that the clouds missed by the model have, on average, a small impact on the observed SWD.

3.3.4 Hit cases: in all situations

We now focus on the hit cases, which are the most frequent and contribute the most to the overall errors. We investi-

gate how in these cases the errors depend on the AROME cloud regimes and satellite cloud types. Figure 8a shows the monthly bias and relative frequency as well as the contribution to the total bias for the hit cases over 2020. It appears that AROME overestimates the SWD for almost all CRs, except for CR0 in all the months and CR4 and CR7 in some months. The largest positive bias is for CR3, with values up to 93 W m^{-2}. Figure 8b shows the same behavior for almost all cloud types, except for FC. Such a positive bias could be explained both by a systematic underestimation of the cloud fraction and/or by an underestimation of the cloud optical thickness. Since we do not have an estimate of the cloud fraction, it is difficult to conclude. Indeed, the evaluation of the cloud fraction at such high spatial and temporal resolutions over a large domain remains a challenge.

To go further, Fig. 9 shows the bias for each cloud regime and four ranges of forecasted cloud fraction. At low cloud fraction (i.e., less than 10 %), the bias, in addition to being the highest for almost all cloud regimes, is positive for all cloud regimes. This is not surprising since when the cloud fraction is low in the model, if the cloud fraction is not correct, it is most likely to be underestimated, resulting in a positive bias. For a high cloud fraction (more than 95 %), the bias remains positive for CR2, CR3, CR5 and CR6, despite the fact that in this case, if the cloud fraction is not correct, it is most likely to be overestimated, which would lead to a negative bias. This suggests that for these cloud regimes, errors are not only governed by cloud fraction errors.

This preliminary analysis highlights errors that can be attributed to cloud fraction errors. Since we do not have access to a reliable cloud fraction observation for the AROME resolution and domain, we do not pursue the evaluation under all cloudy conditions. Instead, from now on we focus on situations where the AROME cloud fraction is close to unity, which means that positive biases at least cannot be attributed to an underestimation of the cloud fraction.

3.3.5 Hit cases: in overcast situations

As explained above, we now focus on overcast situations. In practice, we consider the hit cases for which the AROME cloud fraction is larger than 95 %, which corresponds to 61 % of the hit cases and 40 % of all the cases. The frequency of overcast situations for each cloud regime is shown in Fig. 9 (black numbers in %). In practice, these proportions are largely the same when the overcast threshold is set between 95 % and 99 %. The first effect of this overcast sub-selection is to change the annual bias, leading to a nearly zero bias (1.1 compared to 24 W m^{-2} before). This suggests that part of the overall positive bias may be due to errors in cloud fractions or optical thickness that is too low under partial cloudiness. In contrast, the SDE is barely reduced (101 vs 110 W m^{-2}), showing that the overcast cases still deserve attention and that the nearly zero bias results from error compensations.
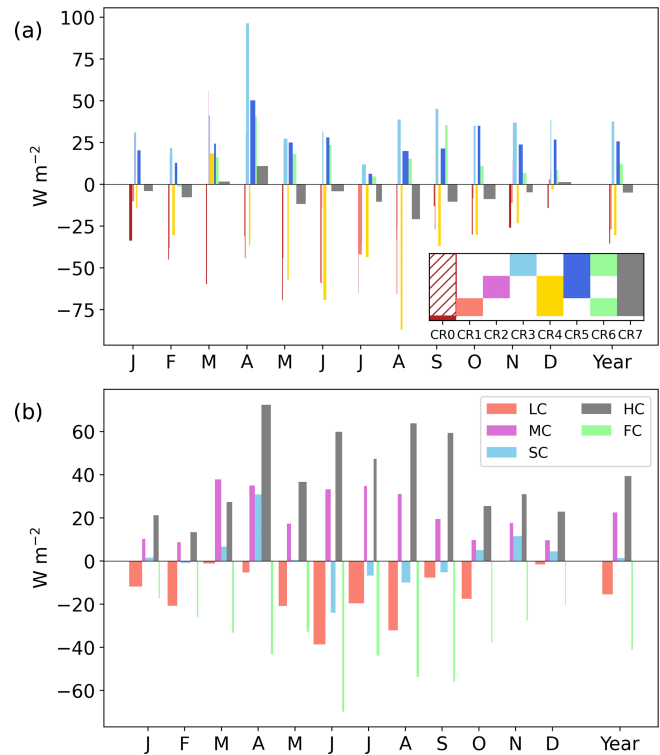

Figure 10. Monthly mean SWD bias (bar height, in W m^{-2}) and relative frequency (bar width) for **(a)** all modeled cloud regimes and **(b)** all observed cloud types, in overcast situations, during the year 2020. The total contribution is the bar surface.

In this section, we investigate how the errors vary with the AROME cloud regimes and satellite cloud types.

We start by distinguishing these overcast hit cases in terms of modeled cloud regime or observed cloud type in the satellite classification. Figure 10a shows the 2020 monthly bias, relative frequency and contribution to total bias.

When the situations are sorted according to the AROME cloud regime, the high clouds (CR3 and CR5) are systematically associated with a positive bias throughout the year, with values up to 100 W m^{-2}. Since these two cloud regimes correspond to 21 % of the cases, this results in a significant positive contribution to the bias. In contrast, the bias for the low clouds (CR1 and CR4) is negative with a more pronounced seasonal cycle, characterized by a stronger bias in summer up to −80 W m^{-2}. Fog cases are associated with negative biases with an annual bias of −25 W m^{-2} and a higher frequency in January. The annual bias is consistent with the already mentioned delay in fog dissipation and the optical depth that is too thick, related to the excess of water content and droplet concentration in the fogs simulated by AROME, as pointed out by Antoine et al. (2023).

When satellite cloud types are used (Fig. 10b), again we obtain a positive bias for HC, with values up to 70 W m^{-2}; a bias of variable sign for SC; and a persistent negative bias for LC, with values up to −40 W m^{-2}. The bias is always neg-

ative for FC. This is consistent with the fact that this cloud type probably corresponds to situations with a cloud fraction lower than 100 %, meaning that the cloud fraction, if not correct, is overestimated in AROME. Note that satellites with passive instruments cannot detect low clouds when a high cloud layer is present, and therefore the modeled cloud regimes and observed cloud types are not directly comparable.

The results are essentially the same when the cloud fraction threshold for defining the cloud regimes, applied independently over each vertical slice of the troposphere as explained in Sect. 2.2.3, is set to 1 %, 2 %, 5 % or 10 %.

These results, consistent between the AROME and satellite classifications, highlight that although on average the SWD bias is small under overcast conditions, it results from the compensation of large and systematic errors, positive for high clouds and negative for low clouds. This also explains why the SDE remains large compared to the bias.

To further investigate the error distribution for each cloud type, it is useful to examine the CSI for the AROME cloud regimes in overcast situations. Figure 11 shows the CSI distribution for all cloud regimes in the model and in the observations. For CR0, CR1, CR4, CR6 and CR7, i.e., for the cloud regimes which have a non-zero cloud fraction in the lower atmosphere, the model has too many low CSI values below 0.1 compared to the observation. For CR1, and CR4, the model does not have enough values greater than 0.6. These two findings suggest that in overcast situations, the optically thick low clouds are too thick in AROME and that the model does not have enough optically thin low clouds. This explains the overall negative bias for these cloud regimes. For CR3, CR5 and CR6, the model has too many high values (between 0.8 and 1 for CR3, between 0.5 and 0.9 for CR5, and between 0.6 and 1 for CR6) and for CR3 and CR5 not enough low values. This suggests that high clouds are overall optically too thin in AROME. Even though the model does not have CSI values greater than 1, while the observations do, the bias is positive for these cloud regimes, as seen in Fig. 10a. This positive bias is not due to a potentially too small cloud fraction in the model, as only overcast situations in the model are selected.

To further investigate the SDE associated with each cloud regime, Fig. 12 shows the distribution of SWD errors for all AROME cloud regimes. For each CR, the SDE is high compared to the mean flux, in particular for CR2, CR4, CR5 and CR6. Interestingly, it shows that for all cloud regimes the mean biases result from both positive and negative contributions, indicating that multiple sources of errors are involved. The same is obtained for the distribution of SWD errors for observed cloud type in the satellite classification (not shown). This suggests that improving the mean bias of individual cloud regimes would not necessarily imply much better forecasts. It also implies that more detailed observations are needed to better understand these errors and their sources.

To summarize, the errors in overcast conditions depend on the cloud regimes. Low clouds seem on average optically too thick, although the negative bias may be due to an overestimation of the cloud fraction in overcast situations in the model. In contrast, simulated high clouds are often optically too thin. Although it would be interesting to evaluate the model over a longer period, the fact that our results are consistent for each month of 2020 suggest that they are not specific to this particular year.

4 Discussion

In this section, we first address the cloud fraction issue and provide a critical analysis of the satellite cloud mask and cloud type. We then investigate potential sources of error in AROME that could explain the observed SWD errors.

4.1 Limitation of the observations

4.1.1 Cloud fraction

In this study we did not evaluate cloud fraction, so we could not attribute SWD errors to potential cloud fraction errors. Indeed, evaluating the cloud fraction at AROME resolution over a large domain is challenging because spatially and temporally resolved cloud fraction observations at such spatial resolution are not common.

The cloud fraction of AROME at 2.5 km horizontal resolution has already been evaluated at a larger timescale between 2000 and 2018 with the 0.05° COMET and 0.25° CLARA satellite products by Lucas-Picher et al. (2022). They show that in summer, AROME underestimates the cloud fraction over land, resulting in an overestimation of SWD, while it overestimates the cloud fraction in winter and spring. SWD is also overestimated in spring and fall, although less than in summer. Like Lucas-Picher et al. (2022), we found a SWD positive bias for every month of the year (Fig. 5a), even in winter and spring when the cloud fraction is possibly overestimated. This suggests that sources of error other than the cloud fraction are responsible for the positive SWD bias and that the underestimation of the cloud fraction in summer further accentuates the bias.

Satellite products at finer resolution should be used to analyze cloud fraction errors in AROME at 1.3 km resolution over the whole year of 2020, such as the daily MODIS product (Ackerman et al., 2008), although this product cannot capture the targeted hourly resolution. An alternative to satellite observations would be to use ground observations from instrumented sites, allowing evaluation at a finer scale. Cloud fraction can be estimated from global and diffuse shortwave broadband measurements (Long et al., 2006), all-sky imaging systems (Pfister et al., 2003), or remote sensing instruments such as radar, lidar and microwave radiometers (e.g., Illingworth et al., 2007).
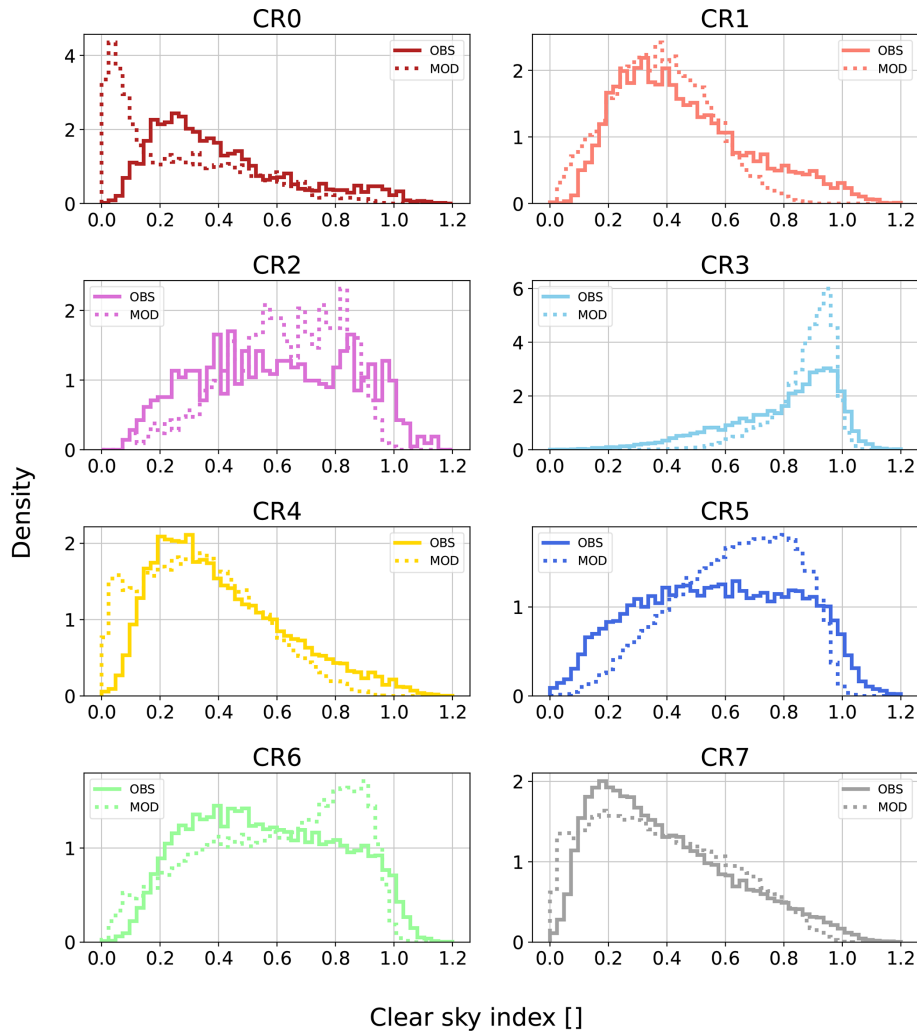
Figure 11. Distribution of clear-sky index for CR0, CR1, CR2, CR3, CR4, CR5, CR6 and CR7 in AROME and in the observations when the SZA is less than 70°.

However, the cloud fractions derived from different observations generally differ (Long et al., 2006; Wagner and Kleiss, 2016), and more critically, the cloud fraction is somehow loosely defined, so that the observed cloud fraction does not necessarily match the model definition (Brooks et al., 2005). Above all, assessing the performance based solely on a few sites would not be consistent with the evaluation strategy adopted in this study.

4.1.2 Cloud detection by satellite

In this paper, several hints suggest that some clouds are not detected by the satellite product, such as the asymmetry between the frequency of clear skies in the model and in the observations (Sect. 2.2.3) or between the frequency of false alarm and miss cases (Sect. 3.2). In addition, the temporal variability of SWD under clear sky is much larger in the ob-

servations than in the model (not shown). This questions the reliability of the satellite cloud mask used.

The likely non-detection of clouds may have an impact on our results. For the correct negative cases, this could explain a SWD positive bias in AROME, with clouds present in reality but not detected, and an overestimation of the frequency of correct negative cases. Likewise, it may lead to an underestimation of the hit cases' frequency, in addition to not taking into account some optically thin real clouds in the error calculations. However, the impact on the hit cases is probably limited due to their high relative frequency compared to the probably low relative occurrence of non-detection. In the future, a more reliable cloud detection could be based on ground observations from remote sensing instruments or high-frequency global and diffuse SWD measurements (Long and Ackerman, 2000).
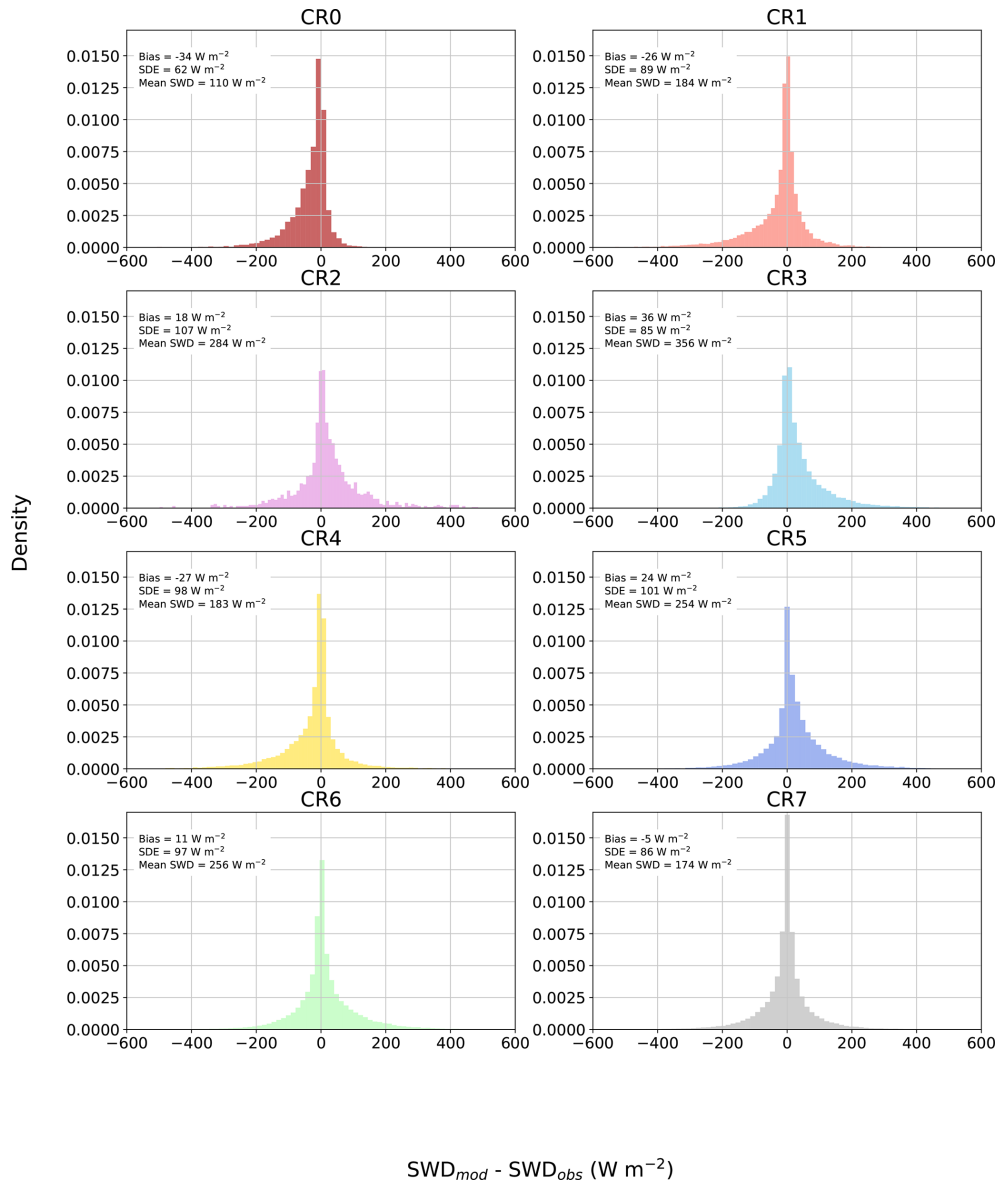
Figure 12. Distribution of SWD errors (bias and SDE indicated) for CR0, CR1, CR2, CR3, CR4, CR5, CR6 and CR7 cloud regimes in overcast situations.

It should be noted that there may also be cases of clouds detected but not present in reality (LeGléau and Kerdraon, 2019) but that the impact is probably negligible in our study.

4.2 Cross-comparison between the cloud regimes and the cloud types

To assess the consistency between simulated cloud regimes (CRs) and observed cloud types (CTs) and analyze the matches between the model and the observations, a cross-comparison is shown in Fig. 13. It displays the distribution of cloud types for each cloud regime and, conversely, for the hit cases in overcast situations. Recall that the parallel between

cloud regime and cloud type is not direct since satellite products do not see what is under an optically thick cloud.

For low clouds, Fig. 13a shows that for CR0, CR4 and mainly for CR1, LC is most often observed. In contrast, Fig. 13b shows that when LC is observed, CR7 and CR6 are most often simulated, more than CR0, CR1 and CR4. CR2, CR3 and CR5 remain very rare in this case. The relative high frequencies of CR6 when LCs are observed (18.8 %) and of LCs when CR6 is simulated (50.9 %) can be explained by the non-detection of optically thin high clouds. Note that in Sect. 2.2.3, we have shown that CR7 clouds are far too frequent in the model compared to observations (HC) and that it is therefore not surprising to find an excessive occurrence of
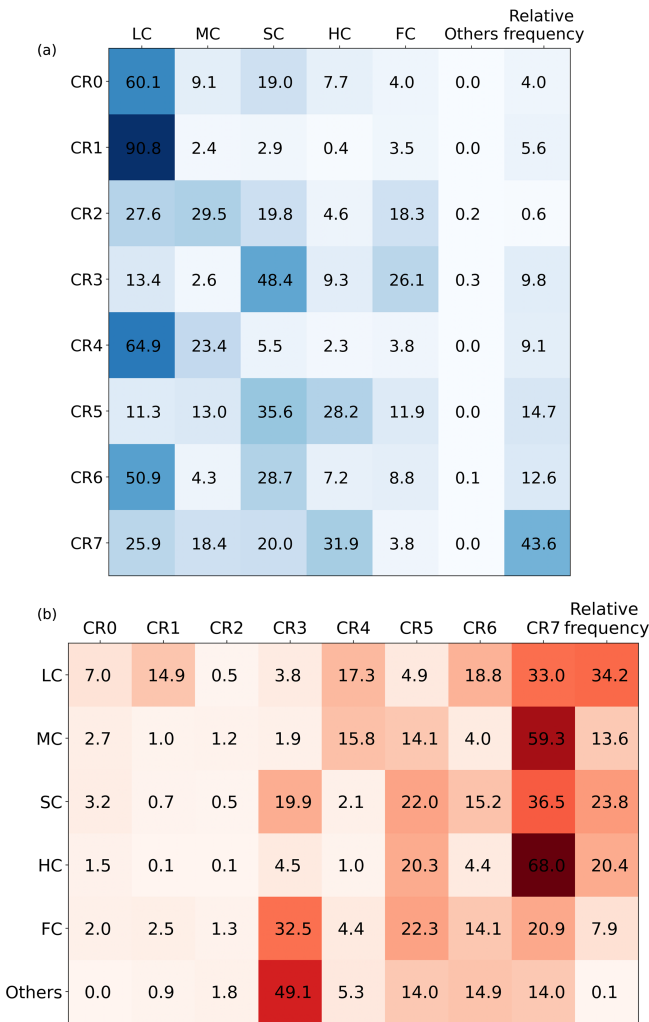
(a)

	LC	MC	SC	HC	FC	Others	Relative frequency
CR0	60.1	9.1	19.0	7.7	4.0	0.0	4.0
CR1	90.8	2.4	2.9	0.4	3.5	0.0	5.6
CR2	27.6	29.5	19.8	4.6	18.3	0.2	0.6
CR3	13.4	2.6	48.4	9.3	26.1	0.3	9.8
CR4	64.9	23.4	5.5	2.3	3.8	0.0	9.1
CR5	11.3	13.0	35.6	28.2	11.9	0.0	14.7
CR6	50.9	4.3	28.7	7.2	8.8	0.1	12.6
CR7	25.9	18.4	20.0	31.9	3.8	0.0	43.6

(b)

	CR0	CR1	CR2	CR3	CR4	CR5	CR6	CR7	Relative frequency
LC	7.0	14.9	0.5	3.8	17.3	4.9	18.8	33.0	34.2
MC	2.7	1.0	1.2	1.9	15.8	14.1	4.0	59.3	13.6
SC	3.2	0.7	0.5	19.9	2.1	22.0	15.2	36.5	23.8
HC	1.5	0.1	0.1	4.5	1.0	20.3	4.4	68.0	20.4
FC	2.0	2.5	1.3	32.5	4.4	22.3	14.1	20.9	7.9
Others	0.0	0.9	1.8	49.1	5.3	14.0	14.9	14.0	0.1

Figure 13. Cross-comparison of cloud regime/cloud type (in %) in hit cases. **(a)** For each CR, the relative frequency of each CT. The last column is the relative frequency of each CR for all hits in overcast situations. The sum of each row is equal to 1. **(b)** For each CT, the relative frequency for each CR. The last column is the relative frequency of each CT over all hits in overcast situations. The sum of each row is equal to 1.

CR7 in some cloud types. Even so, this suggests that for low clouds, the cloud type is in reasonable agreement with the model, and thus the negative bias of SWD found in Sect. 3.3 is actually related to poorly simulated low clouds. The study of fog remains limited by satellite because the satellite product includes fog in low clouds (LeGleau, 2019), as fog and low stratus are difficult to distinguish (Bendix et al., 2005).

For optically thin high clouds, Fig. 13a shows that for CR3, SCs (48.4 %) and FCs (26.1 %) are mostly observed, which means a good match for optically thin high clouds since the distinction between SC and FC is questionable. Indeed, very thin cirrus are often classified as fractional clouds (LeGleau, 2019). Conversely, in Fig. 13b for SC, mostly CR7

(36.5 %), CR5 (22.0 %) and CR3 (19.9 %) are simulated, so the relative frequency of CR7, as for LC, seems too high. For FC, CR3 is mostly simulated (32.5 %).

For optically thick high clouds that most likely correspond to CR5, CR7 and HC, Fig. 13a shows that for CR5, SC and HC are mainly observed (63.8 % when added together), much more than LC, MC and FC. For HC, CR5 (20.3 %) and CR7 (68.0 %) are mainly simulated, while few CR0, CR1 and CR4 clouds are simulated. This means that we also have a relatively good match for high opaque clouds (HCs) and geometrically thick high clouds in the model (CR5, CR7). Thus, for high clouds, the model cloud regimes are in reasonable agreement with the observed cloud type, even though CR7 is too frequent in the model. This suggests that the positive SWD bias found in Sect. 3.3 is indeed related to high clouds.

In summary, there is generally a good correlation between the modeled cloud regime and the observed cloud type, although the match is not perfect. When the model predicts low clouds, mostly low clouds are observed, and when the model predicts high clouds, mostly semi-transparent and opaque clouds are observed. However, CR7 seems too frequent, with, in particular, too many occurrences when LCs are observed. Note, however, that some of the errors may also come from the fact that we compare instantaneous satellite products to hourly mean values of the model.

4.3 Investigating AROME errors

We now identify potential sources of error in AROME that could explain the biases highlighted in Sect. 3.3. Wurtz et al. (2021) pointed out that in AROME, the ice and snow contents of the anvils of mesoscale convective systems are too small. Their spatial extent is also too small, which they attributed to excessive snowfall velocities in AROME, resulting from a poor parametrization of the ice particle size distribution, an issue already reported by Taufour et al. (2018). Wurtz et al. (2023) improved the treatment of snow in AROME, a correction that could help increase the snow mass and thus reduce the positive SWD bias for high clouds if snow is properly accounted for in the radiative code.

Another explanation for the positive SWD bias for high clouds could be that snow (which is one of the hydrometeors simulated by the microphysical scheme) is currently not taken into account in the AROME radiative code. Yet, on average over 2020, the total snow mass is 1.6 times that of cloud ice, meaning that a significant mass is neglected in the AROME radiative calculations. This is especially true for CR3, CR5 and CR7 where the snow mass dominates both the cloud liquid and cloud ice masses (not shown). In practice, it is recommended to include snow in radiative calculations, as snow has a significant radiative impact on the SWD as shown in the IFS model (Li et al., 2014a) and CMIP simulations (Li et al., 2014b, 2022), at least in regions with high precipitation and/or convective activity. Applying the correction developed by Wurtz et al. (2023) and taking into account

the radiative effect of snow could reduce the positive SWD bias for high clouds found in this study. Note however that it could also deteriorate the bias for low clouds that are already too opaque (e.g., CR4 in winter).

Apart from the treatment of snow and ice, SWD errors have often been attributed to liquid water path (LWP) errors. Evaluation of LWP in AROME could provide information on LWP errors and help understand the SWD negative bias in overcast situations. However, evaluating the LWP at AROME resolution over a large domain and a full year is challenging since geostationary satellite LWP products, such as the NWC SAF product, remain very limited because they rely on passive instruments. To investigate SWD errors due to LWP errors, a case study could be conducted, such as Ahlgrimm and Forbes (2012), who identified LWP errors using microwave radiometer measurements that could explain the SWD positive bias in overcast low cloud situations in the IFS model. For instance, observations from the SIRTA supersite on the Saclay plateau (Chiriaco et al., 2018) could be used to better separate the contributions of variables such as cloud fraction, liquid water path and cloud droplet effective radius. Polar-orbiting satellites with active measurements onboard (e.g., CloudSat and CALIPSO, Stephens et al., 2018) could also be used to analyze the contributions of LWP and IWP (ice water path) errors, but their spatial and temporal coverage is very limited for evaluating the performance of NWP models at hourly and kilometric resolutions.

Errors in the representation of the mixed phase were also highlighted by Forbes and Ahlgrimm (2014) in the IFS model and Barrett et al. (2017) in five operational NWP models including the IFS model, as well as Engdahl et al. (2020) in HARMONIE-AROME. They reported an underestimation of the supercooled liquid water content in boundary layer clouds. This would likely result in an overestimation of SWD (Hogan et al., 2003), which could explain the positive SWD bias for the clouds involved, namely CR2, CR4 and CR5. Although this error source is not consistent with the average negative SWD bias we found for CR4 in overcast conditions, it may account for some positive errors (see Fig. 12) for CR4 and participate in the positive bias for CR2 and CR5.

To conclude, several sources of error have been highlighted in the literature, some of which may contribute to the SWD errors reported in our study. Further investigations with more advanced observations should be used to overcome the limitations of the observations used in this study.

5 Conclusions

In this study, we performed a detailed evaluation of the 24 h SWD forecasts of the French NWP model AROME at 1.3 km horizontal resolution, comparing a full year of hourly forecasts with in situ SWD measurements from the pyranometer network operated by Météo-France. A preliminary analysis showed that errors mainly occur when clouds are present in the model and in the observations, while erroneously predicted and missed clouds contribute less to the overall errors, as these situations are less frequent. Missed clouds and erroneously predicted clouds mainly correspond to clouds with a low impact on the SWD. Errors in cloudy situations, which have a positive bias overall, can also result from errors in the simulated cloud fraction or in the cloud optical thickness. Since errors in the cloud fraction are difficult to evaluate over a large domain, we limited our study to overcast situations in the model, implying that the SWD overestimation cannot be attributed to an underestimation of the cloud fraction. In such overcast conditions, the overall bias is close to zero. We then quantified the SWD errors for different cloud regimes, corresponding to different cloud altitudes. In doing so, we found a systematic SWD negative bias for low clouds and a systematic SWD positive bias for high clouds, consistent throughout the year, which essentially compensate to the near zero bias. In addition to these systematic deviations, we found unsystematic errors with significant SDE for all cloud regimes, which is critical for the solar energy sector. Note that this study was based on only 1 year, and even if the results seem to be robust with similar SWD errors through the year, it might be relevant to extend this study to several years. A cross-comparison between cloud regimes and cloud types showed relatively good agreement between the model and observations, especially for low clouds, confirming that the negative bias of SWD is indeed related to low clouds and the positive bias of the SWD is indeed related to high clouds. We pointed out that the positive bias of ice clouds may be due to the failure to account for snow in the AROME radiation code or to the too low snow content of ice clouds, issues that could be addressed in the future. Other sources of SWD errors have been mentioned, such as LWP or mixed-phase representation errors.

Our results also suggest that some clouds are not detected by the satellite, highlighting the need for more detailed cloud observations to go further in error assessment. In addition, efforts should be made to evaluate the cloud fraction at AROME resolution over a large domain to fully characterize the performance of AROME for SWD forecasts. This may be addressed using large networks of ceilometers or more complete shortwave radiation measurements. To better understand which physical properties of clouds cause SWD errors, further evaluations that distinguish cloud fraction errors from errors in the vertical distributions of condensed water and cloud particle effective radius are needed and should be based on highly instrumented sites. Although the study focused on AROME, the presented methodology can be applied to any NWP model, and the detailed evaluation can provide valuable physical information about the model performance, paving the way for future model improvement.

References

ACCORD: http://www.umr-cnrm.fr/accord/, last access: 11 January 2024.

Ackerman, S. A., Holz, R., Frey, R., Eloranta, E., Maddux, B., and McGill, M.: Cloud detection with MODIS. Part II: validation, J. Atmos. Ocean. Tech., 25, 1073–1086, 2008.

Ahlgrimm, M. and Forbes, R.: The Impact of Low Clouds on Surface Shortwave Radiation in the ECMWF Model, Mon. Weather Rev., 140, 3783–3794, https://doi.org/10.1175/mwr-d-11-00316.1, 2012.

Amodei, M. and Stein, J.: Deterministic and fuzzy verification methods for a hierarchy of numerical models, Meteorol. Appl., 16, 191–203, https://doi.org/10.1002/met.101, 2009.

Antoine, S., Honnert, R., Seity, Y., Vié, B., Burnet, F., and Martinet, P.: Evaluation of an improved AROME configuration for fog forecasts during the SOFOG3D campaign, Weather Forecast., 38, 1605–1620, https://doi.org/10.1175/WAF-D-22-0215.1, 2023.

Antonanzas, J., Osorio, N., Escobar, R., Urraca, R., de Pison, F. M., and Antonanzas-Torres, F.: Review of photovoltaic power forecasting, Sol. Energy, 136, 78–111, https://doi.org/10.1016/j.solener.2016.06.069, 2016.

Barrett, A. I., Hogan, R. J., and Forbes, R. M.: Why are mixed-phase altocumulus clouds poorly predicted by large-scale models? Part 2. Vertical resolution sensitivity and parameterization, J. Geophys. Res.-Atmos., 122, 9927–9944, https://doi.org/10.1002/2016jd026322, 2017.

Bendix, J., Thies, B., Cermak, J., and Nauß, T.: Ground Fog Detection from Space Based on MODIS Daytime Data – A Feasibility Study, Weather Forecast., 20, 989–1005, https://doi.org/10.1175/WAF886.1, 2005.

Benedetti, A., Morcrette, J.-J., Boucher, O., Dethof, A., Engelen, R. J., Fisher, M., Flentje, H., Huneeus, N., Jones, L., Kaiser, J. W., Kinne, S., Mangold, A., Razinger, M., Simmons, A. J., and Suttie, M.: Aerosol analysis and forecast in the European Centre for Medium-Range Weather Forecasts Integrated Forecast System: 2. Data assimilation, J. Geophys. Res., 114, D13205, https://doi.org/10.1029/2008JD011115, 2009.

Bengtsson, L., Andrae, U., Aspelien, T., Batrak, Y., Calvo, J., de Rooy, W., Gleeson, E., Hansen-Sass, B., Homleid, M., Hortal, M., Ivarsson, K., Lenderink, G., Niemelä, S., Nielsen, K. P., Onvlee, J., Rontu, L., Samuelsson, P., Muñoz, D. S., Subias, A., Tijm, S., Toll, V., Yang, X., and Køltzow, M. Ø.: The HARMONIE–AROME model configuration in the ALADIN–HIRLAM NWP system, Mon. Weather Rev., 145, 1919–1935, 2017.

Betti, A., Blanc, P., David, M., Saint-Drenan, Y.-M., Driesse, A., Freeman, J., Fritz, R., Gueymard, C., Habte, A., Höller, R., Huang, J., Kazantzidis, A., Kleissl, J., Köhler, C., Landelius, T., Lara-Fanego, V., Lorenz, E., Lauret, P., Martin, L., Mehos, M., Meyer, R., Myers, D., Nielsen, K. P., Perez, R., Peruchena, C. F., Polo, J., Renné, D., Ramírez, L., Remund, J., Ruiz-Arias, J. A., Sengupta, M., Silva, M., Spieldenner, D., Stoffel, T., Suri, M., Wilbert, S., Wilcox, S., Vignola, F., Wang, P., Xie, Y., and Zarzalejo, L. F.: Best Practices Handbook for the Collection and Use of Solar Resource Data for Solar Energy Applications: Third Edition, Tech. rep., International Energy Agency, https://iea-pvps.org/key-topics/best-practices-handbook-for-the-collection-and-use-of-solar-resource-data-for-

solar-energy-applications-third-edition/ (last access: 31 January 2024), 2021.

Bougeault, P. and Lacarrere, P.: Parameterization of orography-induced turbulence in a mesobeta–scale model, Mon. Weather Rev., 117, 1872–1890, 1989.

Bozzo, A., Benedetti, A., Flemming, J., Kipling, Z., and Rémy, S.: An aerosol climatology for global models based on the tropospheric aerosol scheme in the Integrated Forecasting System of ECMWF, Geosci. Model Dev., 13, 1007–1034, https://doi.org/10.5194/gmd-13-1007-2020, 2020.

Brooks, M. E., Hogan, R. J., and Illingworth, A. J.: Parameterizing the difference in cloud fraction defined by area and by volume as observed with radar and lidar, J. Atmos. Sci., 62, 2248–2260, 2005.

Brousseau, P., Seity, Y., Ricard, D., and Léger, J.: Improvement of the forecast of convective activity from the AROME-France system, Q. J. Roy. Meteor. Soc., 142, 2231–2243, https://doi.org/10.1002/qj.2822, 2016.

Chiriaco, M., Dupont, J.-C., Bastin, S., Badosa, J., Lopez, J., Haeffelin, M., Chepfer, H., and Guzman, R.: ReOBS: a new approach to synthesize long-term multi-variable dataset and application to the SIRTA supersite, Earth Syst. Sci. Data, 10, 919–940, https://doi.org/10.5194/essd-10-919-2018, 2018.

Chu, Y., Li, M., Pedro, H. T., and Coimbra, C. F.: A network of sky imagers for spatial solar irradiance assessment, Renew. Energ., 187, 1009–1019, https://doi.org/10.1016/j.renene.2022.01.032, 2022.

Copernicus Atmosphere Monitoring Service: Copernicus Atmosphere Data Store, https://atmosphere.copernicus.eu/ last access: 11 January 2024

Cros, S., Badosa, J., Szantaï, A., and Haeffelin, M.: Reliability Predictors for Solar Irradiance Satellite-Based Forecast, Energies, 13, 5566, https://doi.org/10.3390/en13215566, 2020.

Cuxart, J., Bougeault, P., and Redelsperger, J.-L.: A turbulence scheme allowing for mesoscale and large-eddy simulations, Q. J. Roy. Meteor. Soc., 126, 1–30, https://doi.org/10.1002/qj.49712656202, 2000.

Das, U. K., Tey, K. S., Seyedmahmoudian, M., Mekhilef, S., Idris, M. Y. I., Deventer, W. V., Horan, B., and Stojcevski, A.: Forecasting of photovoltaic power generation and model optimization: A review, Renew. Sustain. Energ. Rev., 81, 912–928, https://doi.org/10.1016/j.rser.2017.08.017, 2018.

Dubus, L., Brayshaw, D. J., Huertas-Hernando, D., Radu, D., Sharp, J., Zappa, W., and Stoop, L. P.: Towards a future-proof climate database for European energy system studies, Environ. Res. Lett., 17, 121001, https://doi.org/10.1088/1748-9326/aca1d3, 2022.

Engdahl, B. J. K., Thompson, G., and Bengtsson, L.: Improving the representation of supercooled liquid water in the HARMONIE-AROME weather forecast model, Tellus A, 72, 1–18, 2020.

Forbes, R. M. and Ahlgrimm, M.: On the Representation of High-Latitude Boundary Layer Mixed-Phase Cloud in the ECMWF Global Model, Mon. Weather Rev., 142, 3425–3445, https://doi.org/10.1175/mwr-d-13-00325.1, 2014.

Fouquart, Y. and Bonnel, B.: Computations of solar heating of the Earth's atmosphere: A new parameterization, Beitraege zur Physik der Atmosphaere, 53, 35–60, 1980.

Gueymard, C. A.: Cloud and albedo enhancement impacts on solar irradiance using high-frequency measurements from thermopile and photodiode radiometers. Part 1: Impacts on global horizontal irradiance, Sol. Energ., 153, 755–765, 2017.

Hogan, R. J., Francis, P., Flentje, H., Illingworth, A., Quante, M., and Pelon, J.: Characteristics of mixed-phase clouds. I: Lidar, radar and aircraft observations from CLARE'98, Q. J. Roy. Meteor. Soc., 129, 2089–2116, https://doi.org/10.1256/rj.01.208, 2003.

ICARE On-line Data Archive, https://www.icare.univ-lille.fr/, last access: 11 January 2024.

Illingworth, A. J., Hogan, R. J., O'Connor, E., Bouniol, D., Brooks, M. E., Delanoé, J., Donovan, D. P., Eastment, J. D., Gaussiat, N., Goddard, J. W. F., Haeffelin, M., Baltink, H. K., Krasnov, O. A., Pelon, J., Piriou, J.-M., Protat, A., Russchenberg, H. W. J., Seifert, A., Tompkins, A. M., van Zadelhoff, G.-J., Vinit, F., Willén, U., Wilson, D. R., and Wrench, C. L.: Cloudnet, B. Am. Meteorol. Soc., 88, 883–898, https://doi.org/10.1175/BAMS-88-6-883, 2007.

International Energy Agency: Etat du photovolatïque en France, Tech. rep., Agence de l'Environnement et de la Maîtrise de l'Energie and International Energy Agency, 2019.

Kosmopoulos, P. G., Kazadzis, S., Taylor, M., Athanasopoulou, E., Speyer, O., Raptis, P. I., Marinou, E., Proestakis, E., Solomos, S., Gerasopoulos, E., Amiridis, V., Bais, A., and Kontoes, C.: Dust impact on surface solar irradiance assessed with model simulations, satellite observations and ground-based measurements, Atmos. Meas. Tech., 10, 2435–2453, https://doi.org/10.5194/amt-10-2435-2017, 2017.

Köhler, C., Steiner, A., Saint-Drenan, Y.-M., Ernst, D., Bergmann-Dick, A., Zirkelbach, M., Bouallègue, Z. B., Metzinger, I., and Ritter, B.: Critical weather situations for renewable energies – Part B: Low stratus risk for solar power, Renew. Energ., 101, 794–803, https://doi.org/10.1016/j.renene.2016.09.002, 2017.

Lac, C., Chaboureau, J.-P., Masson, V., Pinty, J.-P., Tulet, P., Escobar, J., Leriche, M., Barthe, C., Aouizerats, B., Augros, C., Aumond, P., Auguste, F., Bechtold, P., Berthet, S., Bielli, S., Bosseur, F., Caumont, O., Cohard, J.-M., Colin, J., Couvreux, F., Cuxart, J., Delautier, G., Dauhut, T., Ducrocq, V., Filippi, J.-B., Gazen, D., Geoffroy, O., Gheusi, F., Honnert, R., Lafore, J.-P., Lebeaupin Brossier, C., Libois, Q., Lunet, T., Mari, C., Maric, T., Mascart, P., Mogé, M., Molinié, G., Nuissier, O., Pantillon, F., Peyrillé, P., Pergaud, J., Perraud, E., Pianezze, J., Redelsperger, J.-L., Ricard, D., Richard, E., Riette, S., Rodier, Q., Schoetter, R., Seyfried, L., Stein, J., Suhre, K., Taufour, M., Thouron, O., Turner, S., Verrelle, A., Vié, B., Visentin, F., Vionnet, V., and Wautelet, P.: Overview of the Meso-NH model version 5.4 and its applications, Geosci. Model Dev., 11, 1929–1969, https://doi.org/10.5194/gmd-11-1929-2018, 2018.

Lafore, J. P., Stein, J., Asencio, N., Bougeault, P., Ducrocq, V., Duron, J., Fischer, C., Héreil, P., Mascart, P., Masson, V., Pinty, J. P., Redelsperger, J. L., Richard, E., and de Arellano, J. V.-G.: The Meso-NH Atmospheric Simulation System. Part I: adiabatic formulation and control simulations, Ann. Geophys., 16, 90–109, https://doi.org/10.1007/s00585-997-0090-6, 1998.

LeGleau, H.: User Manual for the Cloud Product Processors of the NWC/GEO: Science Part, Tech. rep., EUMETSAT NWCSAF, 2019.

LeGléau, H. and Kerdraon, G.: Scientific and Validation report for the Cloud Product Processors of the NWC/GEO, Tech. rep., EU-METSAT NWCSAT, 2019.

Li, J.-L., Forbes, R., Waliser, D., Stephens, G., and Lee, S.: Characterizing the radiative impacts of precipitating snow in the ECMWF integrated forecast system global model, J. Geophys. Res.-Atmos., 119, 9626–9637, 2014a.

Li, J.-L., Lee, W.-L., Waliser, D., David Neelin, J., Stachnik, J. P., and Lee, T.: Cloud-precipitation-radiation-dynamics interaction in global climate models: A snow and radiation interaction sensitivity experiment, J. Geophys. Res.-Atmos., 119, 3809–3824, 2014b.

Li, J.-L. F., Xu, K.-M., Lee, W.-L., Jiang, J. H., Fetzer, E., Stephens, G., Wang, Y.-H., and Yu, J.-Y.: Exploring Radiation Biases Over the Tropical and Subtropical Oceans Based on Treatments of Frozen-Hydrometeor Radiative Properties in CMIP6 Models, J. Geophys. Res.-Atmos., 127, e2021JD035976, https://doi.org/10.1029/2021JD035976, 2022.

Logothetis, S.-A., Salamalikis, V., Wilbert, S., Remund, J., Zarzalejo, L. F., Xie, Y., Nouri, B., Ntavelis, E., Nou, J., Hendrikx, N., Visser, L., Sengupta, M., Pó, M., Chauvin, R., Grieu, S., Blum, N., van Sark, W., and Kazantzidis, A.: Benchmarking of solar irradiance nowcast performance derived from all-sky imagers, Renew. Energ., 199, 246–261, https://doi.org/10.1016/j.renene.2022.08.127, 2022.

Long, C. N. and Ackerman, T. P.: Identification of clear skies from broadband pyranometer measurements and calculation of downwelling shortwave cloud effects, J. Geophys. Res.-Atmos., 105, 15609–15626, https://doi.org/10.1029/2000jd900077, 2000.

Long, C. N., Ackerman, T. P., Gaustad, K. L., and Cole, J. N. S.: Estimation of fractional sky cover from broadband shortwave radiometer measurements, J. Geophys. Res., 111, D11204, https://doi.org/10.1029/2005jd006475, 2006.

Lucas-Picher, P., Brisson, E., Caillaud, C., Alias, A., Nabat, P., Lemonsu, A., Poncet, N., Hernandez, V. E. C., Michau, Y., Doury, A., Monteiro, D., and Somot, S.: Evaluation of the convection-permitting regional climate model CNRM-AROME41t1 over northwestern Europe, Research Square [preprint], https://doi.org/10.21203/rs.3.rs-1393181/v1, 2022.

Magnaldo, M.-A., Libois, Q., Riette, S., and Lac, C.: AROME forecasts of surface shortwave downward radiation for year 2020, Zenodo [data set], https://doi.org/10.5281/zenodo.7928622, 2023.

Masson, V., Le Moigne, P., Martin, E., Faroux, S., Alias, A., Alkama, R., Belamari, S., Barbu, A., Boone, A., Bouyssel, F., Brousseau, P., Brun, E., Calvet, J.-C., Carrer, D., Decharme, B., Delire, C., Donier, S., Essaouini, K., Gibelin, A.-L., Giordani, H., Habets, F., Jidane, M., Kerdraon, G., Kourzeneva, E., Lafaysse, M., Lafont, S., Lebeaupin Brossier, C., Lemonsu, A., Mahfouf, J.-F., Marguinaud, P., Mokhtari, M., Morin, S., Pigeon, G., Salgado, R., Seity, Y., Taillefer, F., Tanguy, G., Tulet, P., Vincendon, B., Vionnet, V., and Voldoire, A.: The SURFEXv7.2 land and ocean surface platform for coupled or offline simulation of earth surface variables and fluxes, Geosci. Model Dev., 6, 929–960, https://doi.org/10.5194/gmd-6-929-2013, 2013.

Météo-France: Météo France Données Publiques, https://donneespubliques.meteofrance.fr/?fond=produit&id_produit=298&id_rubrique=32, last access: 11 January 2024.

Mlawer, E. J., Taubman, S. J., Brown, P. D., Iacono, M. J., and Clough, S. A.: Radiative transfer for inhomogeneous atmospheres: RRTM, a validated correlated-k model for the longwave, J. Geophys. Res.-Atmos., 102, 16663–16682, 1997.

Morcrette, J.-J.: Assessment of the ECMWF model cloudiness and surface radiation fields at the ARM SGP site, Mon. Weather Rev., 130, 257–277, 2002.

Morcrette, J.-J., Boucher, O., Jones, L., Salmond, D., Bechtold, P., Beljaars, A., Benedetti, A., Bonet, A., Kaiser, J. W., Razinger, M., Schulz, M., Serrar, S., Simmons, A. J., Sofiev, M., Suttie, M., Tompkins, A. M., and Untch, A.: Aerosol analysis and forecast in the European Centre for Medium-Range Weather Forecasts Integrated Forecast System: Forward modeling, J. Geophys. Res., 114, D06206, https://doi.org/10.1029/2008JD011235, 2009.

Nielsen, K. P. and Gleeson, E.: Using shortwave radiation to evaluate the HARMONIE-AROME weather model, Atmosphere, 9, 163, https://doi.org/10.3390/atmos9050163, 2018.

Nouri, B., Kuhn, P., Wilbert, S., Hanrieder, N., Prahl, C., Zarzalejo, L., Kazantzidis, A., Blanc, P., and Pitz-Paal, R.: Cloud height and tracking accuracy of three all sky imager systems for individual clouds, Sol. Energ., 177, 213–228, https://doi.org/10.1016/j.solener.2018.10.079, 2019a.

Nouri, B., Wilbert, S., Segura, L., Kuhn, P., Hanrieder, N., Kazantzidis, A., Schmidt, T., Zarzalejo, L., Blanc, P., and Pitz-Paal, R.: Determination of cloud transmittance for all sky imager based solar nowcasting, Sol. Energ., 181, 251–263, https://doi.org/10.1016/j.solener.2019.02.004, 2019b.

NWC SAF Documentation, http://www.nwcsaf.org, last access: 11 January 2024.

Perez, R., Lorenz, E., Pelland, S., Beauharnois, M., Knowe, G. V., Hemker, K., Heinemann, D., Remund, J., Müller, S. C., Traunmüller, W., Steinmaurer, G., Pozo, D., Ruiz-Arias, J. A., Lara-Fanego, V., Ramirez-Santigosa, L., Gaston-Romero, M., and Pomares, L. M.: Comparison of numerical weather prediction solar irradiance forecasts in the US, Canada and Europe, Sol. Energ., 94, 305–326, https://doi.org/10.1016/j.solener.2013.05.005, 2013.

Pergaud, J., Masson, V., Malardel, S., and Couvreux, F.: A Parameterization of Dry Thermals and Shallow Cumuli for Mesoscale Numerical Weather Prediction, Bound.-Lay. Meteorol., 132, 83–106, https://doi.org/10.1007/s10546-009-9388-0, 2009.

Pfister, G., McKenzie, R., Liley, J., Thomas, A., Forgan, B., and Long, C. N.: Cloud coverage based on all-sky imaging and its impact on surface solar irradiance, J. Appl. Meteorol. Clim., 42, 1421–1434, 2003.

Raza: On recent advances in PV output power forecast, Sol. Energ., 136, 125–144, https://doi.org/10.1016/j.solener.2016.06.073, 2016.

Rieger, D., Steiner, A., Bachmann, V., Gasch, P., Förstner, J., Deetz, K., Vogel, B., and Vogel, H.: Impact of the 4 April 2014 Saharan dust outbreak on the photovoltaic power generation in Germany, Atmos. Chem. Phys., 17, 13391–13415, https://doi.org/10.5194/acp-17-13391-2017, 2017.

Riette, S. and Lac, C.: A New Framework to Compare Mass-Flux Schemes Within the AROME Numerical Weather Prediction Model, Bound.-Lay. Meteorol., 160, 269–297, https://doi.org/10.1007/s10546-016-0146-9, 2016.

Réseau de transport d'électricité: Panorama de l'électricité renouvelable, Tech. rep., Agence ORE and Enedis and Réseau de transport d'électricité and Syndicat des énergies renouvelables, 2021.

Seity, Y., Brousseau, P., Malardel, S., Hello, G., Bénard, P., Bouttier, F., Lac, C., and Masson, V.: The AROME-France Convective-

Scale Operational Model, Mon. Weather Rev., 139, 976–991, https://doi.org/10.1175/2010MWR3425.1, 2011.

Stein, J. and Stoop, F.: Neighborhood-Based Contingency Tables Including Errors Compensation, Mon. Weather Rev., 147, 329–344, https://doi.org/10.1175/MWR-D-17-0288.1, 2019.

Stephens, G., Winker, D., Pelon, J., Trepte, C., Vane, D., Yuhas, C., L'ecuyer, T., and Lebsock, M.: CloudSat and CALIPSO within the A-Train: Ten years of actively observing the Earth system, B. Am. Meteorol. Soc., 99, 569–581, 2018.

Sun, W., Videen, G., Kato, S., Lin, B., Lukashin, C., and Hu, Y.: A study of subvisual clouds and their radiation effect with a synergy of CERES, MODIS, CALIPSO, and AIRS data, J. Geophys. Res.-Atmos., 116, D22207, https://doi.org/10.1029/2011JD016422, 2011.

Taufour, M., Vié, B., Augros, C., Boudevillain, B., Delanoë, J., Delautier, G., Ducrocq, V., Lac, C., Pinty, J.-P., and Schwarzenböck, A.: Evaluation of the two-moment scheme LIMA based on microphysical observations from the HyMeX campaign, Q. J. Roy. Meteorol. Soc., 144, 1398–1414, 2018.

Tegen, I., Hollrig, P., Chin, M., Fung, I., Jacob, D., and Penner, J.: Contribution of different aerosol species to the global aerosol extinction optical thickness: Estimates from model results, J. Geophys. Res.-Atmos., 102, 23895–23915, https://doi.org/10.1029/97JD01864, 1997.

Tuononen, M., O'Connor, E. J., and Sinclair, V. A.: Evaluating solar radiation forecast uncertainty, Atmos. Chem. Phys., 19, 1985–2000, https://doi.org/10.5194/acp-19-1985-2019, 2019.

Wagner, T. J. and Kleiss, J. M.: Error characteristics of ceilometer-based observations of cloud amount, J. Atmos. Ocean. Tech., 33, 1557–1567, 2016.

Weverberg, K. V., Morcrette, C. J., Petch, J., Klein, S. A., Ma, H.-Y., Zhang, C., Xie, S., Tang, Q., Gustafson, W. I., Qian, Y., Berg, L. K., Liu, Y., Huang, M., Ahlgrimm, M., Forbes, R., Bazile, E., Roehrig, R., Cole, J., Merryfield, W., Lee, W.-S., Cheruy, F., Mellul, L., Wang, Y.-C., Johnson, K., and Thieman, M. M.: CAUSES: Attribution of Surface Radiation Biases in NWP and Climate Models near the U.S. Southern Great Plains, J. Geophys. Res.-Atmos., 123, 3612–3644, https://doi.org/10.1002/2017JD027188, 2018.

Widén, J., Carpman, N., Castellucci, V., Lingfors, D., Olauson, J., Remouit, F., Bergkvist, M., Grabbe, M., and Waters, R.: Variability assessment and forecasting of renewables: A review for solar, wind, wave and tidal resources, Renew. Sustain. Energ. Rev., 44, 356–375, 2015.

Wild, M.: Global dimming and brightening: A review, J. Geophys. Res.-Atmos., 114, D00D16, https://doi.org/10.1029/2008JD011470, 2009.

Wissmeier, U., Buras, R., and Mayer, B.: paNTICA: A Fast 3D Radiative Transfer Scheme to Calculate Surface Solar Irradiance for NWP and LES Models, J. Appl. Meteorol. Clim., 52, 1698–1715, https://doi.org/10.1175/jamc-d-12-0227.1, 2013.

Wurtz, J., Bouniol, D., Vié, B., and Lac, C.: Evaluation of the AROME model's ability to represent ice crystal icing using in situ observations from the HAIC 2015 field campaign, Q. J. Roy. Meteor. Soc., 147, 2796–2817, https://doi.org/10.1002/qj.4100, 2021.

Wurtz, J., Bouniol, D., and Vié, B.: Improvements to the parametrization of snow in AROME in the context of ice crystal icing, Q. J. Roy. Meteor. Soc., https://doi.org/10.1002/qj.4437, 2023.